LETTER

doi:10.1038/nature10793

Abrupt acceleration of a ‘cold’ ultrarelativistic wind from the Crab pulsar

F. A. Aharonian[1,2], S. V. Bogovalov[3] & D. Khangulyan[4]

Pulsars are thought to eject electron–positron winds that energize the surrounding environment, with the formation of a pulsar wind nebula[1]. The pulsar wind originates close to the light cylinder, the surface at which the pulsar co-rotation velocity equals the speed of light, and carries away much of the rotational energy lost by the pulsar. Initially the wind is dominated by electromagnetic energy (Poynting flux) but later this is converted to the kinetic energy of bulk motion[2]. It is unclear exactly where this takes place and to what speed the wind is accelerated. Although some preferred models imply a gradual acceleration over the entire distance from the magnetosphere to the point at which the wind terminates[3,4], a rapid acceleration close to the light cylinder cannot be excluded[5,6]. Here we report that the recent observations of pulsed, very high-energy γ-ray emission from the Crab pulsar[7–9] are explained by the presence of a cold (in the sense of the low energy of the electrons in the frame of the moving plasma) ultrarelativistic wind dominated by kinetic energy. The conversion of the Poynting flux to kinetic energy should take place abruptly in the narrow cylindrical zone of radius between 20 and 50 light-cylinder radii centred on the axis of rotation of the pulsar, and should accelerate the wind to a Lorentz factor of $(0.5\text{–}1.0) \times 10^6$. Although the ultrarelativistic nature of the wind does support the general model of pulsars, the requirement of the very high acceleration of the wind in a narrow zone not far from the light cylinder challenges current models.

The Crab pulsar is one of the brightest γ-ray sources in the sky. Both the light curve and the energy spectrum have been studied[10] in great detail by the Large Area Telescope on board NASA’s Fermi Gamma-ray Space Telescope (Fermi). The phase-averaged spectrum is best fitted by a power law with a photon index of $\alpha = 1.97$ and an exponential cut-off at $E_c = 5.8$ GeV (Fig. 1). Although modified ‘outer gap’ models[11] do allow an extension of the spectrum up to 10 GeV, the detection of pulsed, very high-energy (VHE) γ-ray emission demands a different radiation component. The extrapolation of the fluxes reported by Fermi to the VHE domain as a power law with photon index $\alpha \approx 3.8$, and the claim that such a formal fit is evidence that γ-rays of gigaelectronvolt (GeV) energies have the same magnetospheric origin as those of teraelectronvolt (TeV) energies[8,9,12], in fact requires a drastic revision of basic concepts used at present in magnetospheric models. Moreover, the assumption of a magnetospheric origin for radiation over the entire γ-ray domain contradicts the essentially different light curves reported at GeV (ref. 10) and TeV (refs 7, 9) energies (unless the production sites of these two components are well separated), as well as the apparent tendency of spectral flattening above 100 GeV (Fig. 1).

A natural and more plausible site of production of pulsed VHE γ-rays is the ultrarelativistic wind illuminated by photons originating in the pulsar’s magnetosphere and/or the surface of the neutron star[13]. In the case of the Crab pulsar, the phase-averaged flux of the pulsed (magnetospheric) component exceeds the flux of the thermal emission of the neutron star by two orders of magnitude. The combination of the hard spectral energy distribution of the pulsed emission and the

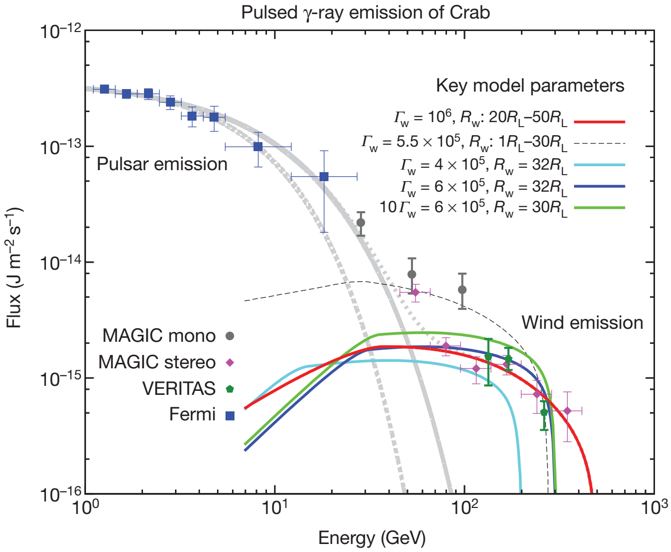

Figure 1 | Spectral energy distribution of γ-ray radiation produced by the pulsar magnetosphere and by the pulsar wind. Symbols show the reported γ-ray fluxes with 1-s.d. error bars[7–10]. Curves show theoretical predictions (this work). The Fermi Large Area Telescope points[10] are best fitted by the function $F_E = 3.8 \times 10^{-13} E^{0.03} \exp[-E/5.8\,\text{GeV}]\,\text{J m}^{-2}\,\text{s}^{-1}$ (dashed grey line). Assuming a slightly harder spectrum in the cut-off region, with $F_E = 3.8 \times 10^{-13} E^{0.03} \exp[-(E/7\,\text{GeV})^{0.85}]\,\text{J m}^{-2}\,\text{s}^{-1}$ (solid grey line), the MAGIC ‘mono’ data points[8] can be explained as well (because of large systematic uncertainties, the mono 100-GeV point, which differs by a factor of three from the flux measured by two MAGIC telescopes in the more reliable stereoscopic regime[9], perhaps ought to be discarded). This spectrum is somewhat harder than that predicted by standard magnetospheric models, but does not challenge them[16–18]. The inverse-Compton γ-ray emission of the cold ultrarelativistic wind[13] can naturally explain the pulsed γ-ray fluxes reported[7,9] above 100 GeV. The solid light-blue, blue and green curves are calculated under the assumption of ‘instant’ acceleration of the wind at the fixed radius R_w. In principle, the acceleration can start earlier, but closer to the light cylinder the acceleration rate should be modest; otherwise it would lead to overproduction of inverse-Compton γ-rays. Earlier acceleration is demonstrated by the dashed black curve, which is calculated under the assumption that acceleration starts at the light cylinder with a rate that increases in proportion with R^3 up to $R_w = 30R_L$, where the Lorenz factor equals 5.5×10^5 (Supplementary Information). The solid red curve corresponds to the case in which the Poynting flux transformation takes place within the $20R_L$–$50R_L$ zone, assuming the wind’s acceleration rate to be independent of distance; the maximum Lorentz factor, achieved at $50R$, is set to 10^6. (The dotted grey line corresponds to the superposition of the red and solid grey lines and shows the transition between the two radiation components.) Because of the decrease in the density of target photons with distance, the main fraction of VHE radiation is produced at around $30R_L$ with a Lorentz factor close to 5×10^5. This explains the general similarity of the red curve to the instant-acceleration curves, apart from in the highest-energy region, where the sharp cut-off of the red curve is shifted to $\sim$500 GeV.

[1]Dublin Institute for Advanced Studies, School of Cosmic Physics, 31 Fitzwilliam Place, Dublin 2, Ireland. [2]Max Planck Institute for Nuclear Physics, Saupfercheckweg 1, 69117 Heidelberg, Germany. [3]National Research Nuclear University (MEPhI), Kashirskoe shosse 31, Moscow, 115409, Russia. [4]Institute of Space and Astronautical Science/JAXA, 3-1-1 Yoshinodai, Chuo-ku, Sagamihara, Kanagawa 252-5210, Japan.

reduction of the Compton cross-section due to the Klein–Nishina effect means that the X-ray band is the main contributor to the Comptonization of the wind. The X-ray flux is well measured up to 100 keV (ref. 14) and therefore the calculations of the inverse-Compton radiation depend basically on the site and the dynamics (speed) of transformation of the Poynting flux to kinetic energy of bulk motion.

We assume that at a distance R_w from the pulsar, the wind is accelerated to the Lorentz factor Γ_w (Fig. 2). Particles of the accelerated wind cannot move purely radially, because the wind should carry both the energy and the angular momentum lost by the pulsar. From the relation between the rotation energy (E_{rot}) and angular momentum (M_{rot}) losses, $\dot{E}_{rot} = \Omega \dot{M}_{rot}$, where Ω is the angular velocity of the rotating sphere and a dot denotes a time derivative, we can define the trajectory of the wind particles. Indeed, each particle of the wind carries energy $\Gamma_w mc^2$ and angular momentum $\Gamma_w m r_\perp v$, where m, $r_\perp$ and v are the particle's mass, lever arm and speed, respectively, and c is the speed of light. Because $\Gamma_w m r_\perp v \Omega = \Gamma_w mc^2$, particles in the accelerated wind move along straight lines, tangent to the light cylinder. Therefore, all photons emitted by the magnetosphere will collide with electrons of the wind at a non-zero angle, θ, resulting in inverse-Compton γ-rays. The γ-ray production efficiency depends on the electron Lorentz factor, the density of the target photons and the interaction angle. Because the cold wind carries almost the entire spin-down luminosity, even a tiny efficiency of about $\kappa \approx 10^{-6}$ should be sufficient to produce detectable γ-rays at an energy flux level of $F_E = \kappa \dot{E}_{rot}/4\pi d^2 \approx 10^{-15}\ \mathrm{J\,m^{-2}\,s^{-1}}$, where $d \approx 6 \times 10^{19}$ m is the distance to the Crab.

Generally, the light curve of the target photons should be reflected in the time structure of the inverse-Compton γ-ray signal; however, they cannot be identical, owing, for example, to the effects related to the specifics of the anisotropic inverse-Compton scattering. More importantly, the geometrical effects may lead to non-negligible differences between the arrival times of the target photon and the secondary γ-ray pulses (Fig. 3). For wind located close to the light cylinder, the γ-ray signal seems shifted in time relative to the reported γ-ray data, by $\Delta t \approx 0.1T$. By contrast, for wind acceleration at $R_w = 30R_L$, the widths and the positions of the predicted and observed γ-ray peaks (P1 and P2, respectively) are in very good agreement. However, whereas in the case of the isotropic wind the predicted P1/P2 flux ratio of the γ-ray signal mimics the X-ray light curve[15] (Fig. 3, black crosses), the reported γ-ray data[7,9] seem to correspond to a smaller ratio, P1/P2 < 1. This can be explained by there being a non-negligible wind anisotropy, which would introduce noticeable corrections to the shape of the γ-ray light curve in general and to the P1/P2 ratio in particular (Fig. 3). The large uncertainties in the present γ-ray data prevent us from a reaching a strong conclusion in this regard, but the improvement of the quality of VHE γ-ray light curves should in future allow the strength and the character of the wind anisotropy to be decisively probed.

GeV γ-rays have a light curve[10] that is essentially different from the reported VHE light curves[7,9]. This can be interpreted as a result of the production of GeV and TeV γ-rays in regions well separated from each other. This conclusion is supported by the spectral energy distribution of the time-averaged GeV and TeV signals. As demonstrated in Fig. 1, the entire γ-ray region can be considered a superposition of two separate components. Indeed, by introducing a new, flat-spectrum VHE component of the Comptonized wind, in addition to the nominal (magnetospheric) GeV component, the reported data in the GeV-to-TeV energy intervals can be smoothly matched.

Although inverse-Compton γ-rays are produced by mono-energetic electrons, the spectral energy distribution of γ-rays in the range of tens to hundreds of GeV is quite flat. This is caused by the combination of effects related to the broad power-law distribution of seed photons and the transition of the Compton cross-section from the Thomson regime to the Klein–Nishina regime. On the other hand, the spectrum is expected to have a very sharp cut-off at $E = \Gamma_w mc^2$. This not only can serve as a distinct feature for the identification of the wind origin of γ-rays, but also should allow us to determine the Lorentz factor of the wind. In fact, the measurements available at present do not allow strong deviation of the Lorentz factor from 5×10^5. We note that the calculations do not depend on the 'magnetization parameter' σ (the ratio of the electromagnetic energy flux to the kinetic energy flux) as long as $R_w \gg R_L$. However, formally we can explain the pulsed VHE emission even for $\sigma \geq 1$. In this case, the acceleration should occur closer to the pulsar ($R_w \propto 1/\sigma^{1/2}$) to compensate for the reduction in the wind's kinetic energy. But in this case, the inverse-Compton γ-ray radiation is expected to have quite different spectral and temporal features.

The above estimates of the location of wind's acceleration site and its Lorentz factor are quite robust, but they are obtained under the assumption that the transformation of the Poynting flux proceeds very quickly, at a specific radius between R_w and $R_w \pm \delta R_w$ with $\delta R_w / R_w \leq 1$. This is not an obvious assumption, but is instead a working hypothesis that the wind acceleration takes place in a narrow zone at the radius $R_w \approx 30R_L$. We cannot a priori exclude the possibility

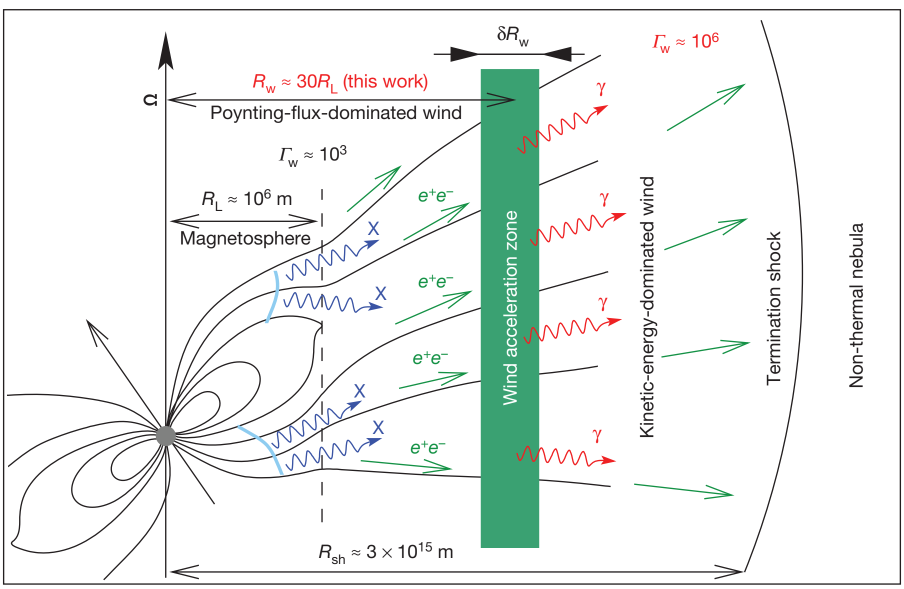

Figure 2 | Complex comprising the pulsar magnetosphere, the ultrarelativistic wind and the pulsar wind nebula. Dense electron (e^-)–positron (e^+) plasma produced in the pulsar magnetosphere by pair creation processes[19] initiates an electron–positron wind at the light cylinder, which has radius $R_L \approx 10^6$ m. Initially, the rotational energy lost by the pulsar, $\dot{E}_{rot} = 5 \times 10^{31}\ \mathrm{J\,s^{-1}}$, is released mainly in the form of electromagnetic energy (Poynting flux) and the wind's Lorentz factor therefore cannot be very large. At a distance R_w, the Poynting flux is converted to the kinetic energy of bulk motion (green zone), leading to an increase in the bulk-motion Lorentz factor to at least[20] $\Gamma_w \approx 10^4$. The termination of the wind by a standing reverse shock at $R_{sh} \approx 3 \times 10^{15}$ m boosts the energy of the electrons to 10^{15} eV and randomizes their pitch angles[2]. The radiative cooling of these electrons through the synchrotron and inverse-Compton processes results in an extended non-thermal source[21–23], the Crab nebula.

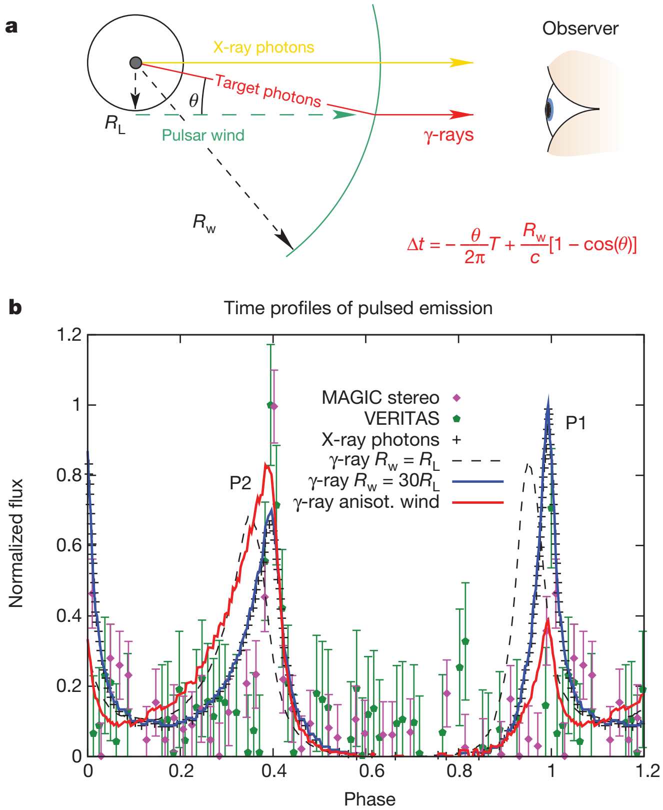

Figure 3 | Formation of the pulsed VHE inverse-Compton γ-ray signal in the wind of the Crab pulsar. **a**, Geometry of the inverse Compton scattering of magnetospheric X-rays by the electron–positron wind. **b**, Theoretical γ-ray light curves of the wind presented together with the reported VHE data[7,9]. The velocity of the accelerated wind is tangential to the light cylinder (the direction of motion of electrons towards the observer is shown by the dashed green arrow). The interaction of electrons with the magnetospheric X-rays occurs predominantly at a distance $R \approx R_w$, where the wind is accelerated. Owing to the decrease in the target photon density with distance, the production of inverse-Compton γ-rays is suppressed at larger distances. The target X-ray photon converted to a VHE γ-ray photon reaches the observer earlier than an 'identical' photon emitted directly towards the observer. Two factors contribute to the time shift, Δt: the up-scattered X-ray photon is emitted by the pulsar earlier, by a time $\theta T/2\pi$, where T is the pulsar period; and it travels an additional path length of $R_w[1 - \cos(\theta)]$. For $R_w \gg R_L$, the time shift is negligibly small: $\Delta t \approx -(T/4\pi)R_L/R_w$. For acceleration of the isotropic pulsar wind at $R_w = 30R_L$, the γ-ray light curve (solid blue line) closely resembles the shape of the measured X-ray light curve[15] (black crosses). For wind accelerated close to the light cylinder, the γ-ray light curve is shifted and somewhat broadened by comparison with wind accelerated at $R_w \gg R_L$. The anisotropy of the wind can also strongly deform the γ-ray light curve; in particular, it can change the ratio of the fluxes corresponding to peaks P1 and P2. The solid red line is calculated for an anisotropy factor proportional to the square of the sine of the angle between the line of sight and the direction of the magnetic momentum. This light curve seems to be in better agreement with the VERITAS[7] and MAGIC[9] points than the light curve corresponding to the fully isotropic wind, although the statistical and systematic uncertainties of observations (only Poisson error bars corresponding to the total count rates are shown on the plot) do not allow a definite conclusion in this regard.

that the wind is gradually accelerated starting from the edge of the magnetosphere, but our numerical calculations show that this cannot be the case (Fig. 1 and Supplementary Information). This is because the gradual acceleration would lead to a large number of high-energy electrons being accelerated close to the light cylinder and, consequently, to the prolific production of inverse-Compton γ-rays, in contradiction with the reported fluxes. Thus, the effective acceleration of the wind should start not much before the radius of $30R_L$ and not much beyond it. Such a case, assuming a linear acceleration rate of $\Gamma(R) = \Gamma_0 + a(R/R_L - 1)$ within the $20R_L$–$50R_L$ radial interval and a maximum Lorenz factor of 10^6 achieved at $50R_L$, is shown in Fig. 1. The corresponding γ-ray spectrum is smoother than the energy spectra predicted in the case of an instant acceleration, and better fits the VHE spectral points (Fig. 1) with the position of the sharp cut-off in the γ-ray spectrum shifted to 500 GeV. Although the wind acceleration within the $20R_L$–$50R_L$ interval seems to be a physically more realistic scenario than an instant acceleration, this is still quite a narrow zone and the acceleration of the wind up to the Lorentz factor of 10^6 is therefore quite abrupt. This conclusion does not agree with those of alternative models, for example the so-called reconnection models of pulsar wind nebulae[3,4] based on the assumption that the transformation of the Poynting flux to kinetic energy of bulk motion is a slow process that takes place over the entire region of the unshocked wind.

Received 5 September; accepted 15 December 2011.

Published online 15 February 2012.

1. Rees, M. J. & Gunn, J. E. The origin of the magnetic field and relativistic particles in the Crab Nebula. *Mon. Not. R. Astron. Soc.* **167,** 1–12 (1974).
2. Kennel, C. F. & Coroniti, F. V. Magnetohydrodynamic model of Crab nebula radiation. *Astrophys. J.* **283,** 710–730 (1984).
3. Coroniti, F. V. Magnetically striped relativistic magnetohydrodynamic winds: the Crab Nebula revisited. *Astrophys. J.* **349,** 538–545 (1990).
4. Lyubarsky, Y. & Kirk, J. G. Reconnection in the striped pulsar wind. *Astrophys. J.* **547,** 437–448 (2001).
5. Vlahakis, N. Ideal magnetohydrodynamic solution to the σ problem in Crab-like pulsar winds and general asymptotic analysis of magnetized outflows. *Astrophys. J.* **600,** 324–337 (2004).
6. Beskin, V. S. & Nokhrina, E. E. The effective acceleration of plasma outflow in the paraboloidal magnetic field. *Mon. Not. R. Astron. Soc.* **367,** 375–386 (2006).
7. Aliu, E, *et al.* Detection of pulsed gamma rays above 100 GeV from the Crab pulsar. *Science* **334,** 69–72 (2011).
8. Aleksić, J. *et al.* Observations of the Crab pulsar between 25 and 100 GeV with the MAGIC I telescope. *Astrophys. J.* **742,** 43 (2011).
9. Aleksić, J. *et al.* Phase-resolved energy spectra of the Crab Pulsar in the range of 50-400 GeV measured with the MAGIC Telescopes. *Astron. Astrophys.* (submitted); preprint at ⟨http://arxiv.org/abs/1109.6124⟩ (2011).
10. Abdo, A. A. *et al. Fermi* Large Area Telescope observations of the Crab pulsar and nebula. *Astrophys. J.* **708,** 1254–1267 (2010).
11. Tang, A. P. S., Takata, J., Jia, J. J. & Cheng, K. S. A revisit of the phase-resolved X-ray and γ-ray spectra of the Crab pulsar. *Astrophys. J.* **676,** 562–572 (2008).
12. Lyutikov, M., Otte, N. & McCann, A. The very-high energy emission from pulsars: a case for inverse Compton scattering. *Astrophys. J.* (submitted); preprint at ⟨http://arxiv.org/abs/1108.3824⟩ (2011).
13. Bogovalov, S. V. & Aharonian, F. A. Very-high-energy γ radiation associated with the unshocked wind of the Crab pulsar. *Mon. Not. R. Astron. Soc.* **313,** 504–514 (2000).
14. Kuiper, L. *et al.* The Crab pulsar in the 0.75–30 MeV range as seen by the CGRO COMPTEL. A coherent high-energy picture from soft X-rays to high-energy γ-rays. *Astron. Astrophys.* **378,** 918–935 (2001).
15. Rots, A. H. *et al.* Absolute timing of the Crab pulsar with the Rossi X-Ray Timing Explorer. *Astrophys. J.* **605,** L129–L132 (2004).
16. Hirotani, K. Outer-gap versus slot-gap models for pulsar high-energy emissions: the case of the Crab pulsar. *Astrophys. J.* **688,** 1254–1267 (2010).
17. Osmanov, Z. & Rieger, F. M. On particle acceleration and very high energy γ-ray emission in Crab-like pulsars. *Astron. Astrophys.* **502,** L25–L28 (2008).
18. Chkheidze, N., Machabeli, G. & Osmanov, Z. On the very high energy spectrum of the Crab pulsar. *Astrophys. J.* **730,** 62 (2011).
19. Sturrock, P. A. A model of pulsars. *Astrophys. J.* **164,** 529–556 (1971).
20. Wilson, D. B. & Rees, M. J. Induced Compton scattering in pulsar winds. *Mon. Not. R. Astron. Soc.* **185,** 297–304 (1978).
21. Gould, R. J. High-energy photons from the Compton-synchrotron process in the Crab nebula. *Phys. Rev. Lett.* **15,** 577–579 (1965).
22. de Jager, O. C. & Harding, A. K. The expected high-energy to ultra-high-energy γ-ray spectrum of the Crab nebula. *Astrophys. J.* **283,** 710–730 (1992).
23. Atoyan, A. M. & Aharonian, F. A. On the mechanisms of γ radiation in the Crab nebula. *Mon. Not. R. Astron. Soc.* **278,** 161–172 (1992).

Supplementary Information is linked to the online version of the paper at www.nature.com/nature.

Acknowledgements We would like to thank J. Cortina, E. de Ona Wilhemi, S. Klepser and N. Otte for information about high-energy γ-ray observations. We also appreciate discussions with F. Rieger, D. Jones and P. Gandhi.

Author Contributions F.A.A., S.V.B. and D.K. jointly contributed in comparable proportions to all aspects of the work, including the calculations and preparation of the manuscript.

Author Information Reprints and permissions information is available at www.nature.com/reprints. The authors declare no competing financial interests. Readers are welcome to comment on the online version of this article at www.nature.com/nature. Correspondence and requests for materials should be addressed to F.A.A. (felix.aharonian@dias.ie).